CONF-8510153--1

SOME ADVANCES IN FRACTURE STUDIES UNDER THE HEAVY-SECTION STEEL TECHNOLOGY PROGRAM*

C. E. Pugh, W. R. Corwin, R. H. Bryan and B. R. Bass

Oak Ridge National Laboratory
Oak Ridge, TN 37831, USA

11th MPA-Seminar 1985, October 10 and 11, 1985

CONF-8510153--1

TI85 018096

ABSTRACT

Recent results are summarized from HSST studies in three major areas that relate to assessing nuclear reactor pressure vessel integrity under pressurized-thermal-shock (PTS) conditions. These areas are irradiation effects on the fracture properties of stainless steel cladding, crack run-arrest behavior under nonisothermal conditions, and fracture behavior of a thick-wall vessel under combined thermal and pressure loadings.

Since a layer of tough stainless steel weld overlay cladding on the interior of a pressure vessel could assist in limiting surface crack extension under PTS conditions, its resistance to radiation embrittlement was examined. A stainless steel overlay cladding, applied by a submerged arc, single-wire, oscillating-electrode method, was irradiated to 2×10^{23} neutrons/m^2 (>1 MeV) at 288°C. Yield strength increases up to 27% and a slight increase in ductility were observed. Charpy V-Notch data showed a ductile-to-brittle transition behavior caused by temperature-dependent failure of the δ-ferrite phase. The type 308 cladding, microstructurally typical of that in reactor pressure vessels, showed very little degradation in either upper-shelf energy or transition temperature due to irradiation.

Crack-arrest behavior of A533 grade B class 1 steel was examined for temperatures extending above the onset of Charpy upper-shelf. Crack-arrest experiments that use wide-plate specimens have shown crack arrest occurring prior to transition to tearing or tensile instability. High values of crack-arrest toughness have been recorded (static values above 400 MPa·$\sqrt{m}$) that are well above the maximum value that safety assessment criteria assume such materials can exhibit.

---

*Research sponsored by Office of Nuclear Regulatory Research, U.S. Nuclear Regulatory Commission under Interagency Agreement DOE 40-551-75 with the U.S. Department of Energy under Contract No. DE-AC05-840R21400 with the Martin Marietta Energy Systems, Inc.

A validation experiment was performed by exposing an intentionally flawed HSST intermediate test vessel to combined pressure and thermal transients. The experiment addressed warm-prestressing phenomena, crack propagation from brittle to ductile regions, and crack stabilization in ductile regions. Test and analysis results are summarized.

1. INTRODUCTION

The Heavy-Section Steel Technology (HSST) program, a major safety program sponsored by the Nuclear Regulatory Commission (NRC) at the Oak Ridge National Laboratory (ORNL), is concerned with the structural integrity of the primary systems [particularly the reactor pressure vessels (RPVs)] of light-water-cooled nuclear power reactors (LWRs). The studies are related to all areas of the technology of materials fabricated into thick-section primary-coolant containment systems of LWRs. The focus is on the behavior and structural integrity of pressure vessels containing crack-like flaws. The program is organized into nine technical tasks and many of the current efforts are directed at establishing the technology and data on which reliable assessments of RPV integrity can be made for hypothetical pressurized-thermal-transient conditions. Base metals, weldments and cladding materials are considered. This paper summarizes some recent results from three of the technical tasks. The three areas are irradiation effects on stainless steel cladding, crack-arrest behavior at high temperatures and toughness levels, and a validation experiment under pressurized-thermal-shock conditions (PTSE-1).

It has been proposed that the existence of a tough surface layer of weld-deposited stainless steel cladding on the interior of a RPV can assist in keeping a short surface flaw from becoming long during a pressurized-thermal-shock (PTS) event, either by impeding the initiation (extension) of a static flaw and/or by arresting a running flaw. To obtain preliminary material-properties data typical of those needed to make such evaluations for LWRs, the HSST program has established a task to obtain data on the degradation (or lack thereof) of the fracture properties of stainless steel weld overlay cladding. A recent review of the literature [1] has indicated that fracture properties of stainless steel weld metal can degrade significantly under irradiation conditions relevant to LWRs. To evaluate this potential degradation, tensile, Charpy V-notch, and precracked Charpy specimens of stainless steel weld overlay cladding were irradiated to about 2×10^{23} neutrons/m^2 (>1 MeV) at 288°C. The results of tensile and Charpy

V-notch tests are reported in Section 2 and compared with the properties of unirradiated cladding.

A primary objective of the HSST crack-arrest studies has been to obtain reliable toughness data and to develop procedures for predicting crack arrest at temperatures approaching the Charpy upper-shelf regime. Early laboratory studies of crack arrest by numerous investigators have led to the use of test specimens that reduce the dynamic effects of a running crack. The current ASTM recommendations on laboratory test procedures are being examined through a round-robin test program [2]. However, these specimens provide limited constraint of deformation in the crack-plane region and a driving force that decreases with crack extension. These factors limit the generation of valid data from these specimens to temperatures below those where arrest is most likely to occur in a PTS scenario. The HSST program is measuring crack-arrest data over an expanded temperature range through thermal-shock [3] and pressurized-thermal-shock [4] tests, which provide validation data under multiaxial transient conditions. The more recent wide-plate tests [5] sponsored by the HSST program are providing the opportunity to obtain a more significant number of data points at affordable costs. Results of these latter experiments are discussed in Section 3 of this paper.

The first HSST pressurized-thermal-shock experiment (PTSE-1) is the most recent of a long succession of fracture-mechanics validation experiments that are on a scale that allows important aspects of the fracture behavior of nuclear reactor pressure vessels to be simulated. Such experiments serve as a means by which theoretical models of fracture behavior can be evaluated for possible application to vessels in nuclear plants. The principal issues of concern in the pressurized-thermal-shock experiments are (1) warm-prestressing phenomena, (2) crack propagation from brittle to ductile regions (3) transient crack stabilization in ductile regions, and (4) crack shape changes in bimetallic zones of clad vessels. PTSE-1, which was designed to investigate the first three of these issues, is summarized in Section 4 of this paper.

2. STAINLESS STEEL CLADDING STUDIES

2.1 MATERIALS AND EXPERIMENTAL PROCEDURE

The specimens in this study were taken from a single laboratory weldment that was fabricated by the automated single-wire oscillating submerged arc procedure for a companion program investigating structural effects of stainless steel cladding on composite four-point bend specimens [6,7]. The weldment consisted of a lower layer of type 309 stainless steel deposited on

a plate of A533 grade B class 1 steel, followed by two upper layers of type 308 stainless steel cladding. The cladding was deposited on plates that were large enough to minimize distortion and to provide an adequate heat sink. The clad plates were then postweld heat treated (PWHT) at 621°C for 40 h to represent commercial practice. Additional details on the welding procedure are discussed in Ref. [8].

The three layers of cladding were applied to provide adequate cladding thickness (~20 mm) to obtain test specimens. This contrasts with typical commercial practice, in which a single layer of overlay approximately 5 mm thick is applied by either multiple wire or strip-cladding submerged arc procedures. The material compositions of each layer of weld metal are given in Table 1. Subsequent metallographic examination showed that the upper layers appeared typical of LWR stainless steel overlay, whereas the lower layer had incurred excessive dilution as a result of base metal melting during welding. Therefore, the data on the microstructurally typical type 308 cladding will be reported here. The upper pass (Fig. 1) shows a distribution of δ-ferrite in an austenite matrix quite typical of microstructures seen in good practice commercial weld overlay cladding in reactor pressure vessels [9]. The effect of the 40-h PWHT on these materials is to partially transform the δ-ferrite to sigma phase. Figure 2 shows that the middle layer similarly contains δ-ferrite dispersed in austenite, but it contains limited regions in which martensite is also present. Subsequent examinations of the fracture surface indicated, however, no noticeable effect of the small amount of martensite present.

Table 1. Chemical composition of overlay weldments

Layer	Content[a] (wt%)												
	C	Cr	Ni	Mo	Mn	Si	Co	Cu	V	Al	Ti	P	S
Lower	0.145	13.46	6.90	0.47	1.47	0.56	0.066	0.14	0.02	0.014	<0.005	0.018	0.01
Middle	0.081	18.52	8.81	0.27	1.47	0.70	0.092	0.10	0.04	0.010	<0.005	0.021	0.01
Upper	0.065	20.01	9.36	0.21	1.49	0.76	0.100	0.09	0.04	0.16	0.006	0.022	0.01

[a]Balance Fe, with Nb, <0.01; Ta, <0.01; As, <0.03; and B, <0.001 for all layers.

Ferrite numbers were measured on the finished Charpy specimens with a Ferrite Scope, which locally measures the percentage of ferromagnetic material in the sample. The specimens consistently had ferrite numbers of 2 to 6 (corresponding roughly to percentages of ferrite).

To assure testing of typical high-quality cladding, tensile and Charpy V-notch specimens were carefully fabricated to be contained as fully as possible within the upper two layers. All specimens were fabricated with the

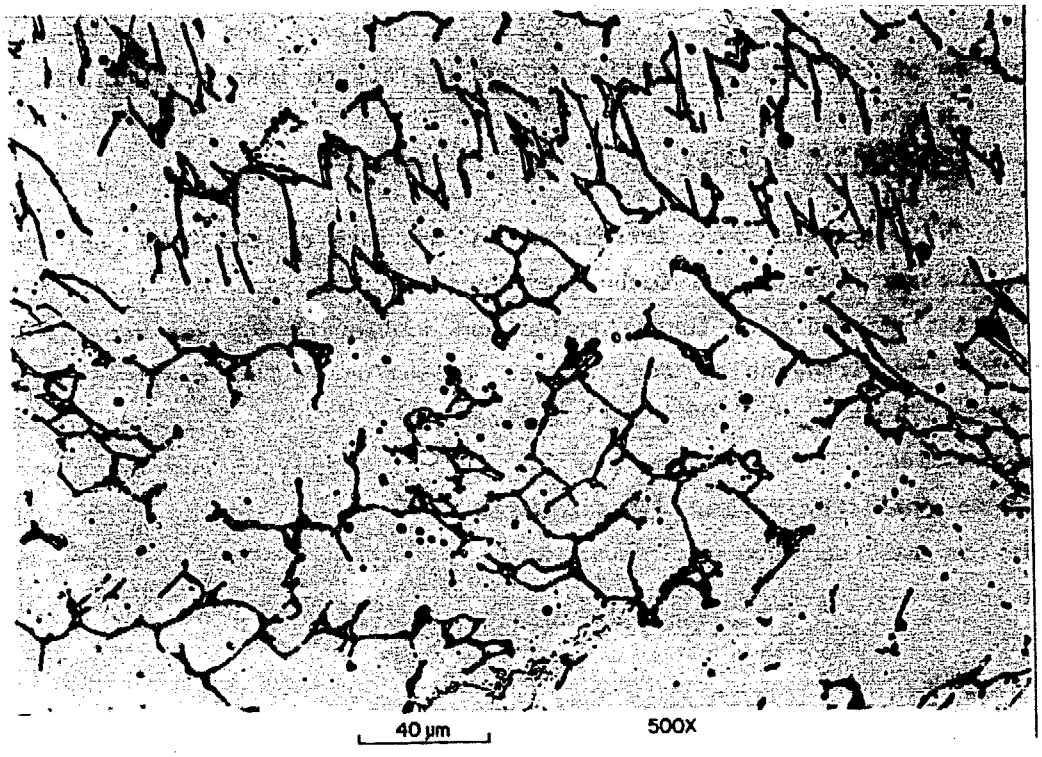

Fig. 1. The microstructure of the top layer of type 308 stainless steel weld overlay is typical of reactor pressure vessel cladding with δ-ferrite in an austenite matrix.

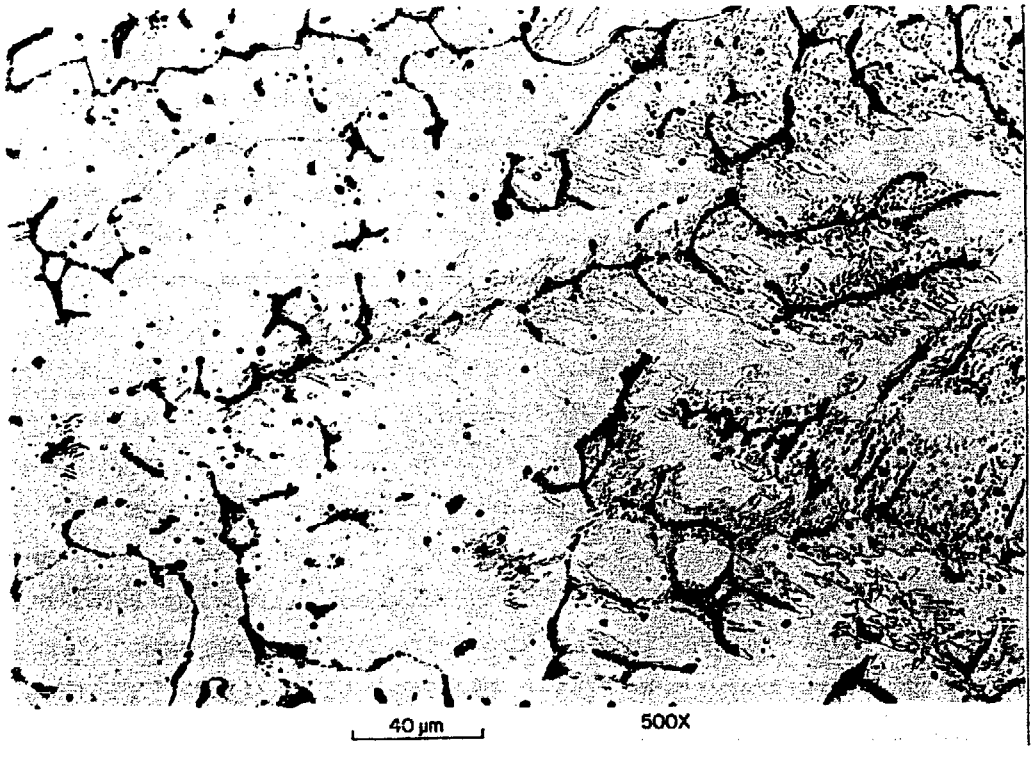

Fig. 2. The middle layer of the overlay (type 308 stainless steel) includes isolated patches of martensite (light gray) in addition to the δ-ferrite in an austenite matrix.

specimen axis parallel to the welding direction. The Charpy specimens were notched on the surface parallel to and nearer the base metal in all cases.

2.2 IRRADIATION HISTORY

The specimens were irradiated in the core of the 2-MW pool reactor at the Nuclear Science and Technology Facility, Buffalo, New York. The capsule was instrumented with thermocouples and dosimeters and was rotated 180° once during the irradiation for fluence balancing. The specimens reached an average fluence of 2.09×10^{23} neutrons/m^2 (>1 MeV) ± 10% during 679 h of irradiation. The fluences are for a calculated spectrum based on Fe, Ni, and Co dosimetry wires. Temperatures were maintained at 288 ± 14°C except for the initial week of irradiation. During that time, temperatures as low as 263°C were recorded.

2.3. RESULTS AND DISCUSSION

Tensile tests were conducted at room temperature, 149, and 288°C. Irradiation increased the yield strength of the type 308 cladding by 5 to 27% (Fig. 3). Surprisingly, the total elongation and reduction of area of the cladding specimens also increased during irradiation (Fig. 4).

The effect of irradiation on the Charpy impact properties of the type 308 weld metal (representative of typical weld overlay cladding) was relatively small (Fig. 5). Only a very slight upward shift in transition temperature (~15°C) and drop in upper shelf (<10%) were observed. It should be noted, for both the control and irradiated specimens, that Charpy curves more typical of ferritic materials than of austenitic stainless steel were observed with respect to the abrupt transition from high- to low-energy fracture. Fracture surfaces of selected specimens were examined in the lower-transition and upper-shelf regions. Macrographs of the irradiated type 308 specimens tested at temperatures low in the transition show flat fracture with clear definition of some of the large grains produced during welding. By comparison, specimens at upper-shelf temperatures produced fracture surfaces more typical of wrought stainless steel with deep shear lips and a dull appearance. Scanning electron microscopy (SEM) of unirradiated specimens tested in the lower-transition and upper-shelf regions clearly show the transition from a cleavage or quasi-cleavage to a fibrous fracture mode (Fig. 6). This behavior compares well with the work of other researchers [10-12], who have shown that fully ductile fracture occurs in as-welded austenitic weld metal as low as 4 K, but that quasi-cleavage can

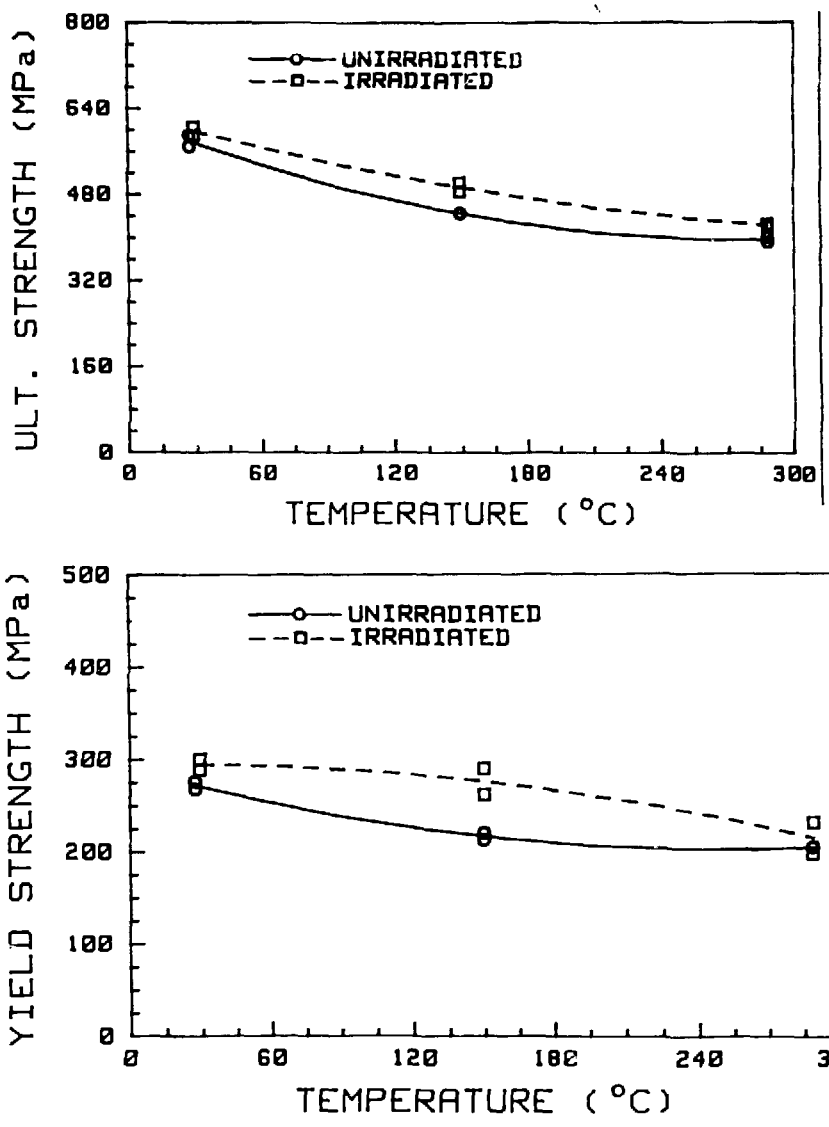

Fig. 3. Effect of irradiation at 288°C to a fluence of 2×10^{23} neutrons/m^2 (>1 MeV) on the tensile strength of the type 308 stainless steel weld metal.

occur in weld metal that has received a PWHT in the temperature range in which carbide precipitation and sigma formation occur.

The minimal effect of irradiation on the impact properties of the good quality type 308 cladding contrasts sharply with the results for the companion poor quality, highly diluted type 309 cladding. The type 309 cladding experienced large upward shifts in transition temperature and drops in the upper shelf energy while maintaining a ferritic transition type behavior similar to that observed in the type 308. This was the result of the atypical microstructure caused by high base metal dilution of the cladding [8]. Since it has been documented that such poor quality cladding exists in some

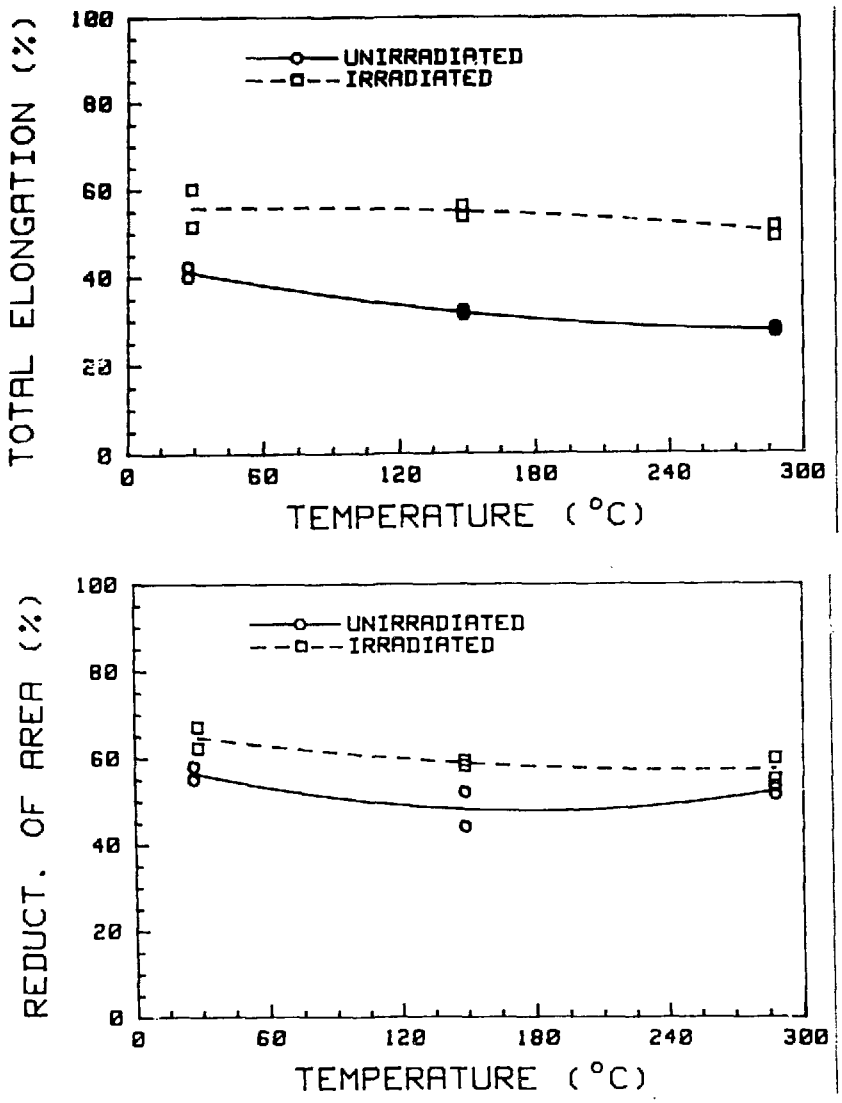

Fig. 4. Effect of irradiation at 288°C to a fluence of 2×10^{23} neutrons/m^2 (>1 MeV) on the tensile ductility of the type 308 stainless steel weld metal.

LWRs [13,14], caution should be exercised in applying the minimal irradiation effects observed in this study for the good quality type 308 cladding.

To further investigate the cause of the ductile-to-brittle transition behavior in an austenitic weld metal, the fracture path within the type 308 weld metal was examined as a function of temperature. Unirradiated Charpy specimens tested at temperatures high and low in the transition region were sectioned and metallographically prepared such that the central plane of the specimen perpendicular to the fracture face was visible, providing a view of the fracture profile.

The reasons for the transition behavior become obvious when the photomicrographs of the lower versus higher temperature tested specimens are

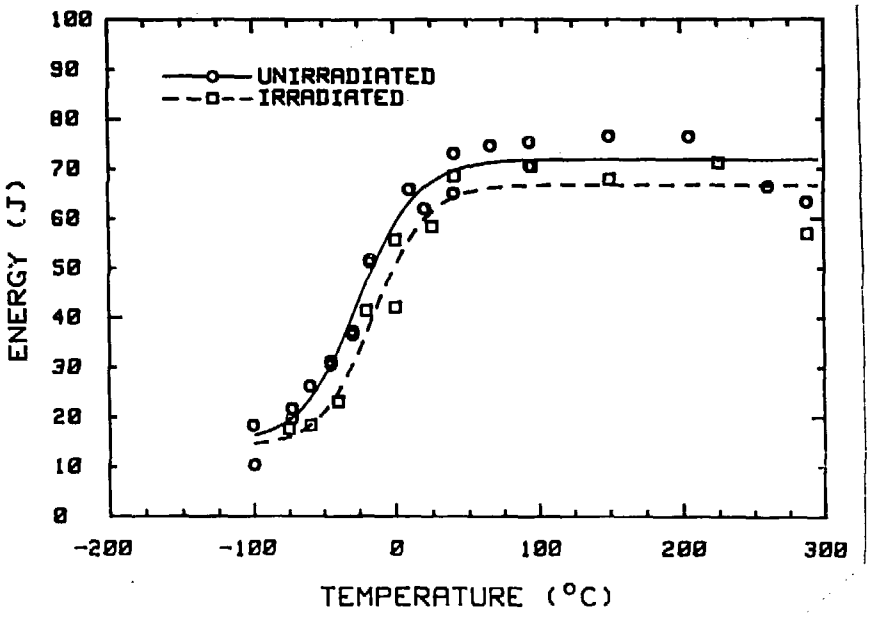

Fig. 5. Effect of irradiation at 288°C to a fluence of 2×10^{23} neutrons/m^2 (>1 MeV) on the Charpy impact energy of type 308 stainless steel cladding.

examined. At the lower temperature (Fig. 7), the fracture path strictly follows the δ-ferrite islands. At a higher magnification (Fig. 8) the sigma phase formed during PWHT can be resolved as dark spots or bands within the δ-ferrite islands. It does not, however, appear that the brittle sigma phase particularly influences the fracture process.

At the higher temperature, the fracture profile within the type 308 stainless steel (Fig. 9) shows clear indications of a dimple rupture failure mode with no preferential δ-ferrite failure.

Based on the fractographic evidence, it appears that for the type 308 stainless steel cladding at upper-shelf temperatures the ferrite is at least as tough as the austenite. The fracture proceeds primarily through the matrix and the ferrite then fails only coincidentally. The mechanism responsible for the typically ferritic type ductile-to-brittle transition observed in our stainless steel cladding has been identified as the low-temperature failure of δ-ferrite regions in the type 308 cladding. This behavior may also explain the rate sensitivity observed by Hawthorne and Watson [15] in their impact testing of stainless steel weldments since the ferritic phases controlling the fracture are inherently rate, as well as temperature, sensitive. If the cladding on the interior of a reactor pressure vessel is to be considered structural in nature, then the potential for its rate sensitivity should also be considered.

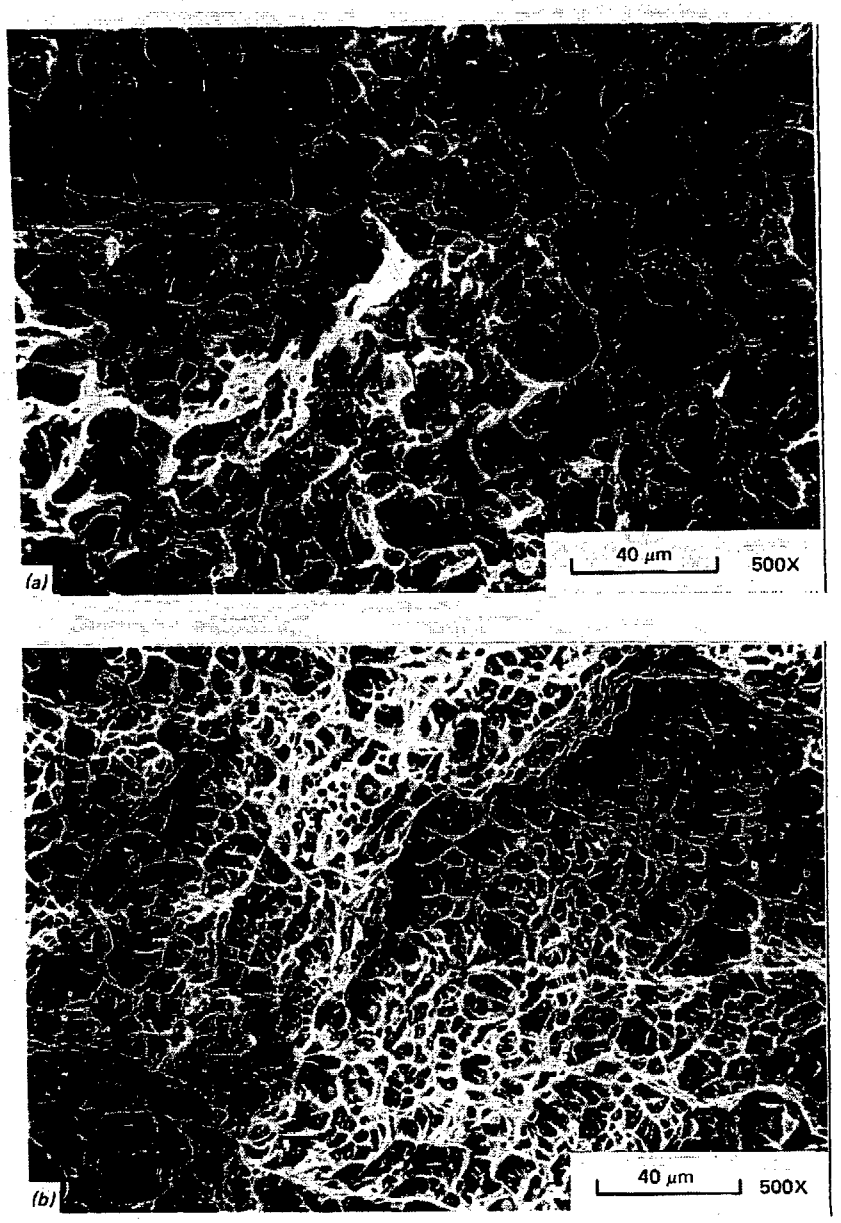

Fig. 6. Scanning electron micrographs of the fracture surfaces of unirradiated type 308 stainless steel cladding Charpy impact specimens. (a) tested at −100°C on the lower shelf, showing predominantly brittle fracture. (b) tested at 150°C on the upper shelf, showing fibrous fracture.

2.4. CONCLUSIONS AND PLANS FOR FURTHER WORK

On the basis of irradiation of one weldment of stainless steel overlay at a temperature and fluence similar to those at end of life for an LWR, very little degradation of the notch-impact toughness displayed by good quality cladding would be expected. In fact, both the tensile strength and the fracture ductility were improved slightly by irradiation. It must be stressed, however, that this is only a single case and that no conclusions,

Fig. 7. Profile of a low-temperature fracture in the type 308 weld shows that the fracture path follows the islands of δ-ferrite.

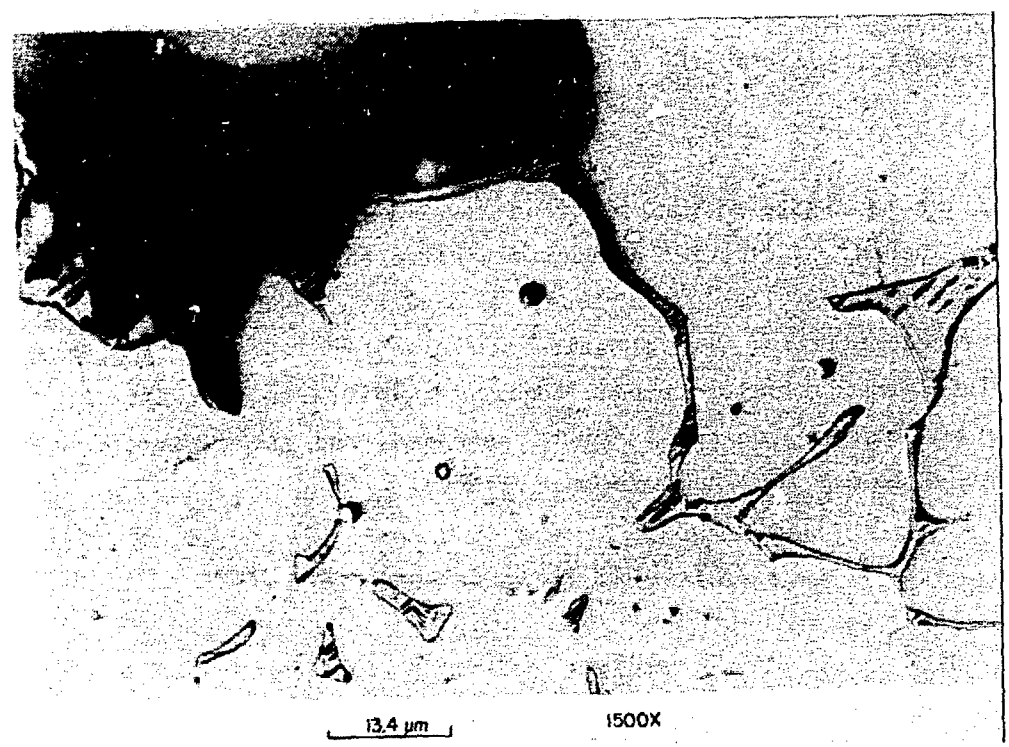

Fig. 8. A higher magnification of the low-temperature fracture profile shows that the sigma phase formed during PWHT, dark lines and dots within δ-ferrite islands, does not appear to influence fracture of the type 308 weld.

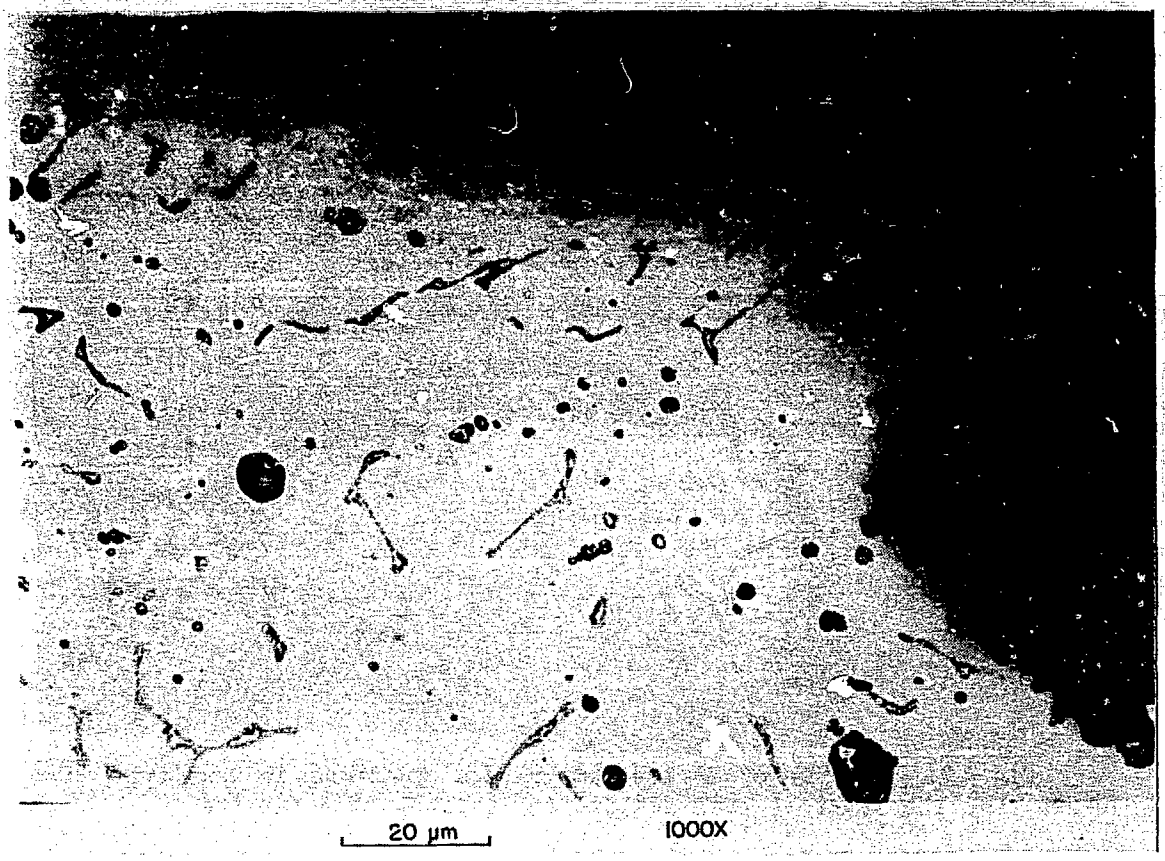

Fig. 9. The profile of the fracture path of type 308 stainless steel tested near the knee of the upper shelf shows that the fracture does not preferentially follow the δ-ferrite (gray patches).

positive or negative, can be drawn regarding welding procedures or compositions leading to material appreciably different from that studied here.

To enlarge this data base, a similar irradiation program has been initiated utilizing 3-wire series arc cladding. In addition, current plans include irradiation of compact tension specimens so that irradiation effects on the fracture toughness can be assessed, and the fluence levels will be extended to 5×10^{23} neutrons/m^2 (>1 MeV).

3. WIDE-PLATE CRACK-ARREST TESTS

HSST crack-arrest studies currently include a series of wide-plate tests of A533 grade B class 1 steel. The tests are designed to measure arrest-toughness values at temperatures ranging above the onset of Charpy upper-shelf behavior. A rising toughness field for crack arrest is achieved by applying a temperature gradient across the span of the plate. The plates are heavily instrumented to record dynamic data, and are tested in a 27 MN

tensile machine at the National Bureau of Standards, Gaithersburg, MD. The first four tests, WP-1.1 through WP-1.4, have been completed.

3.1 SPECIMEN GEOMETRY, MATERIAL PROPERTIES, AND INSTRUMENTATION

The specimen is a 1 × 1 × 0.102 m plate with a single-edge notch that gives an initial crack depth-to-plate width ratio (a/w) of 0.2. Each side of the specimen is side grooved to a depth equal to 12.5% of the plate thickness and the grooves have a 0.25 mm root radius. The initial crack is perpendicular to the rolling direction. The specimen is welded to the pull-plate assembly which has a pin-to-pin length of 9.6 m to minimize stress wave effects. The specimens are taken from the central portion of the 18.73 cm thick HSST plate 13-A of A533 grade B class 1 steel. Properties of this plate include Young's Modulus E = 206.9 GPa, Poisson's Ratio ν = 0.3, thermal expansion coefficient $\alpha = 11 \times 10^{-6}/°C$ and density $\rho = 7850\ kg/m^3$. Temperature-dependent multilinear representations of stress-strain curves for this material are described in Refs. [16,17].

Temperature dependent fracture toughness relations for initiation and arrest, based on small specimen data, are given as follows:

$$K_{Ic} = 51.276 + 51.897\ e^{0.036\ (T\ -\ RT_{NDT})} \tag{1}$$

$$K_{Ia} = 49.957 + 16.878\ e^{0.028738\ (T\ -\ RT_{NDT})} \tag{2}$$

Units for K and T are MPa $\sqrt{m}$ and deg C, respectively. Drop weight and Charpy test data indicate that $RT_{NDT} = -23°C$. The small-specimen K_{Ia} data for this material were obtained by the Battelle Columbus Laboratory (see Ref. [18]), and all other data were obtained by ORNL [19]. Charpy V-Notch results are given in Fig. 10 for specimens taken from the middle of HSST plate 13-A.

Analytical studies have used a dynamic fracture-toughness relation in the following form:

$$K_{ID} = K_{Ia} + A\ (T)\ \dot{a}^2\ , \tag{3}$$

where K_{Ia} is given by Eq. (2) above and

$$A(T) = [329.7 + 16.25\ (T\ -\ RT_{NDT})] \times 10^{-6} \tag{4}$$

or

$$A(T) = [121.71 + 1.296\ (T\ -\ RT_{NDT})] \times 10^{-6}\ , \tag{5}$$

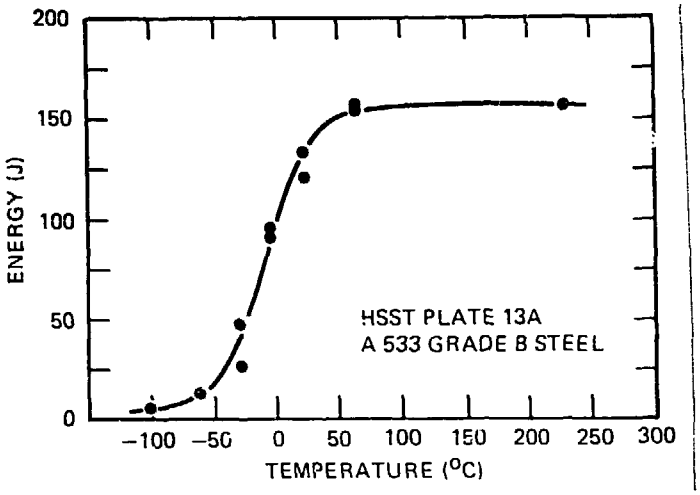

Fig. 10. Charpy V-Notch results for specimens taken from mid-thickness region of HSST-plate 13-A of A533 grade B class 1 steel.

if $(T - RT_{NDT})$ is greater or less than −13.9°C , respectively. Units for K_{ID}, A, $\dot{a}$ and T are MPa$\cdot m^{1/2}$, MPa$\cdot s^2 \cdot m^{-3/2}$, m/s and deg C, respectively. The form of the K_{ID} expression in Eq. (3) and relations for A(T) [Eqs. (4) and (5)] are derived from Ref. [20] by estimating that $RT_{NDT} = -6.1$°C for the material used in that study.

The specimens are instrumented with: (1) thermocouples, (2) strain gages, and (3) crack-opening-displacement (COD) gages. Strain-gage measurements during the test serve to provide dynamic strain-field measurements for determination of crack velocity and to provide far-field strain measurements for determination of loading boundary conditions. Correlation of the COD gage output with pretest and posttest calculations gives an additional check on loading boundary conditions. A series of thermocouples and strain gages are located about 65 mm above the crack plane across the plate.

3.2 MODEL DEFINITION AND ANALYSIS TECHNIQUES

Analyses of the wide-plate experiments have been carried out using both quasistatic and elastodynamic techniques. As stated above, a primary objective of the tests is to obtain K_{Ia} data for temperatures ranging above the onset of the Charpy upper-shelf. To this end, a linear transverse temperature distribution is imposed on the specimen with the crack tip in the cold side of the plate. While the temperature distribution does not impose thermal stresses, the global deformation of the assembly due to thermal strains must be incorporated into the analyses. For finite-element applications, static thermoelastic analyses were performed with the ADINA/ORMGEN/ORVIRT finite element codes (see Refs. [21-23]) to determine the thermal deformation of the plate assembly. These thermal displacements were added to the

nodal point data defining the finite-element model. Generally, the load-line eccentricity caused by the thermal gradients used in the tests elevates the stress intensity factors for the initial crack (a/w = 0.2) by approximately 10 percent.

The postulated crack run-arrest event is dependent upon parameters related to plate geometry, material properties, temperature profile and mechanical loading. After arrest of the crack, depending on the combination of applied load, temperature gradient, and point of arrest, the crack may experience reinitiation in cleavage, stable tearing or unstable ductile tearing combined with tensile instability. To investigate the interactions of the parameters that impact the run-arrest event, both quasistatic and elastodynamic pretest analyses were carried out. For the quasistatic analysis, the computer code WPSTAT [16-17] was developed at ORNL to perform both crack-arrest and crack-stability analyses. The WPSTAT code evaluates static stress-intensity factors as a function of crack length and temperature differential $\Delta T = T_{max} - T_{min}$ across the plate. These factors are computed for fixed-force conditions, $K_I^F(a,\Delta T)$, and for fixed load-pin displacement conditions, $K_I^{DSP}(a,\Delta T)$, by superposing contributions from tension and bending handbook solutions. In addition, WPSTAT categorizes arrested crack lengths in terms of three types of instability limits. First, the instability crack length $a_{rein}(F)$, expressed as a function of the applied load F, defines the limiting value for the arrested crack length below which reinitiation in cleavage may occur. (This may be the case if the initial crack jump is very short, and the temperature of the arrested crack is in the lower-shelf range). The $a_{rein}(F)$ curve is constructed by comparing the $K_I^F(a,\Delta T)$ curve obtained under fixed-force conditions with the $K_{Ic}(T)$ curve of Eq. (1), which is dependent on the location of the crack tip because of the applied temperature gradient.

The limit of the arrested crack length beyond which tensile instability occurs is termed $a_{I1}(F)$. If the crack arrests below the limit for tensile instability and beyond the limit of reinitiation, the possibility exists for the arrest to be stable or for failure to occur by ductile tearing. The region of arrested crack lengths for which tearing instability can occur is defined by $a_{I2}(F)$. Figure 11 illustrates such limits as determined by pretest analysis for the second test, WP-1.2. The dynamic-analysis methods used in this study are described in Ref. [16], where typical detailed results are also shown.

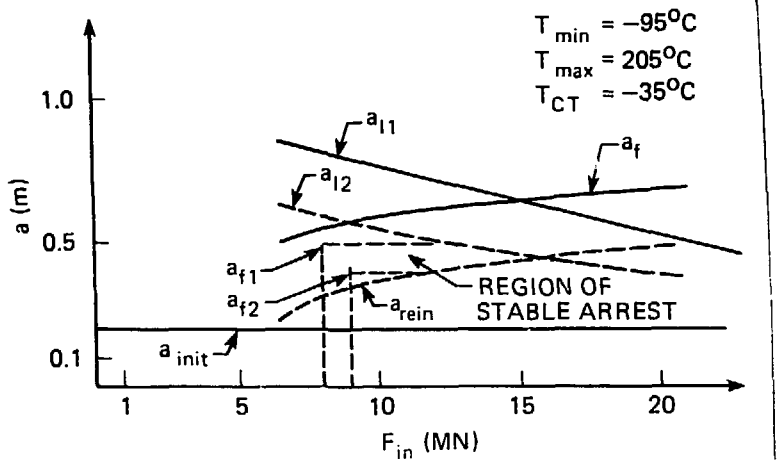

Fig. 11. Results of pretest crack stability analysis of the wide-plate assembly showing limits of reinitiation, tearing and tensile instability for WP-1.2.

3.3 TEST RESULTS

Cleavage initiation was experienced at very high loads in the first two tests, but they exhibited arrest, if for only a small fraction of a second, prior to tearing instability. Test WP-1.2 actually exhibited two such micro-arrest periods. The initiation loads were reduced further for tests WP-1.3 and -1.4. An arrest period of about 2 seconds was experienced in WP-1.3, and the arrest in WP-1.4 was completely stable. Test WP-1.4 was re-initiated by further increase in load to produce a second cleavage initiation-run-arrest event. Table 2 shows the general conditions for these four experiments.

Table 2. Summary of HSST wide-plate crack-arrest tests for A533 grade B class 1 steel

Test No.	Crack location (cm)	Crack temp. (°C)	Initiation load (MN)	Arrest location (cm)	Arrest temp. (°C)	Arrest $T - RT_{NDT}$ (°C)
WP-1.1	20	-60	20.1[a]	50.2	51	74
WP-1.2A	20	-33	18.9	55.5	62	85
WP-1.2B	55.5	62	18.9	64.5	92	115
WP-1.3	20	-51	11.25	48.5	54	77
WP-1.4A	20.7	-63	7.95	44.1	29	52
WP-1.4B	44.1	29	9.72	52.7	60	83

[a]Specimen was warm prestressed by loading to 19 MN while the crack tip drifted from -17 to -9°C.

Crack-arrest toughness values have been determined by various techniques which include detailed static and dynamic analyses as well as handbook techniques. Some of the computed values are shown in Table 3.

Table 3. Computed crack-arrest toughness values from HSST wide-plate tests on A533 grade B class 1 steel

Test no.	Crack-arrest toughness values ($MPa\sqrt{m}$)				
	Static SEN formulas		Alternate static formula[c]	Dynamic FE	
	Displ. control[a]	Load control[b]		Application mode (Ref. 16)	Generation mode (Ref. 16)
WP-1.1	391	813	340	599	NA
WP-1.2A	384	942	349	706.7	440
WP-1.2B	416	1489	419	NA	523
WP-1.3	215	424	185	448	242.8
WP-1.4A	145	248	120	250.9	158
WP-1.4B	331	433	170	NA	396.5

[a] From Ref. [24] (pp. 2.10-2.11) while assuming $a = a_f$ and no further bending occurs due to propagation of the crack

[b] From Ref. [24] (pp. 2.10-2.11) while assuming $a = a_f$ and full bending according to SEN formula when the final crack depth is used.

[c] $K_I = \sigma \left\{ \pi a \sec\left(\frac{\pi a}{2w}\right) \right\}^{1/2}$ from Ref. [25-26], and σ = far-field tensile stress, $a = a_f$ = final crack length, and w = full plate width.

3.4 DISCUSSION

The values labeled in Table 3 as being from an alternate static formula are computed from $K_I = \sigma \left\{ \pi a \sec\left(\frac{\pi a}{2w}\right) \right\}^{1/2}$. This equation is discussed in Refs. [25-26], and the results are plotted in Fig. 12. (The terms in this static formula are defined in a footnote to Table 3.) Figure 12 also includes the K_{IR} curve from Section XI of the ASME Code and the K_{Ia} curve that corresponds to Eq. (2). The trend of the wide-plate test results shows a rapidly increasing toughness at temperatures near and above the onset of the Charpy upper shelf ($T = 55°C$ or $T - RT_{NDT} = 78°C$). The values obtained from tests WP-1.1 through -1.4 extend above the limit (220 $MPa\cdot\sqrt{m}$) of the ASME curve. This observation, that arrest can be expected at these conditions, suggests that the $K_{Ia} = 220$ $MPa\cdot\sqrt{m}$ limit is conservative. Of course, it

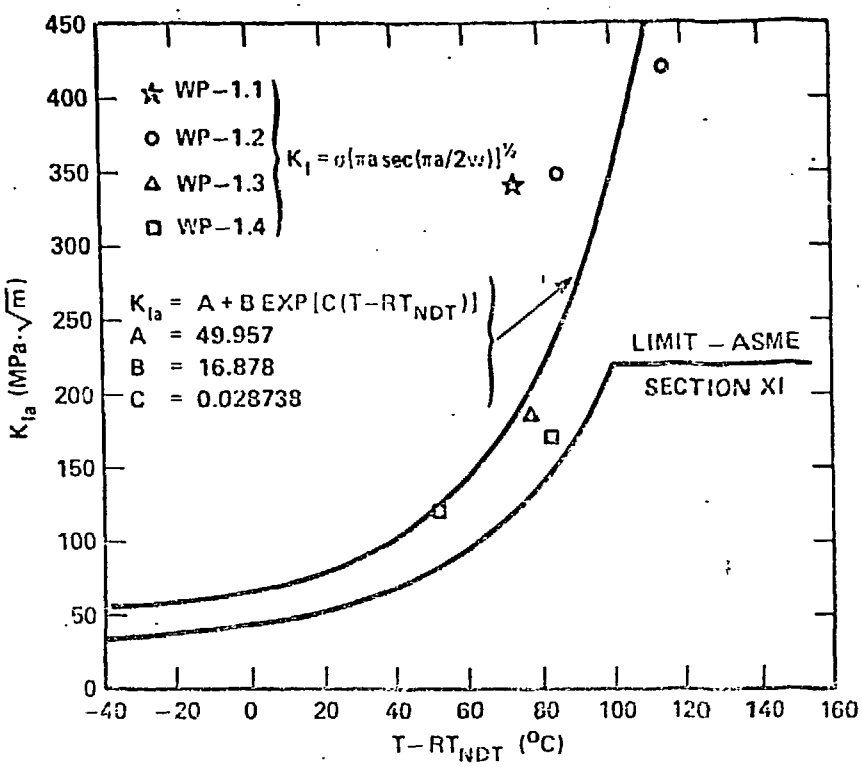

Fig. 12. Wide-plate specimen high-temperature crack-arrest data extend above the ASME limit of 220 MPa·√m.

must be used in conjunction with other analyses of tearing and tensile instability to be complete.

4. PRESSURIZED-THERMAL-SHOCK EXPERIMENT, PTSE-1

4.1 EXPERIMENT DESCRIPTION

The first in a planned series of pressurized-thermal-shock experiments (PTSE) was completed with the externally flawed 148-mm-thick steel vessel. The experiment was performed in a facility constructed at ORNL that allows important aspects of the fracture behavior of PWR vessels to be simulated under postulated PTS conditions. These aspects include warm prestressing and arrest on the upper shelf in prototypically thick sections. The flawed vessel was enclosed in an outer vessel, as shown schematically in Fig. 13, which was electrically heated to bring the test vessel to an initial temperature of about 290°C. A thermal transient is initiated by suddenly injecting chilled water or a methanol-water mixture into the outer vessel. The annulus between the cylindrical surfaces of the two vessels was designed to permit coolant velocities that would produce the appropriate convective

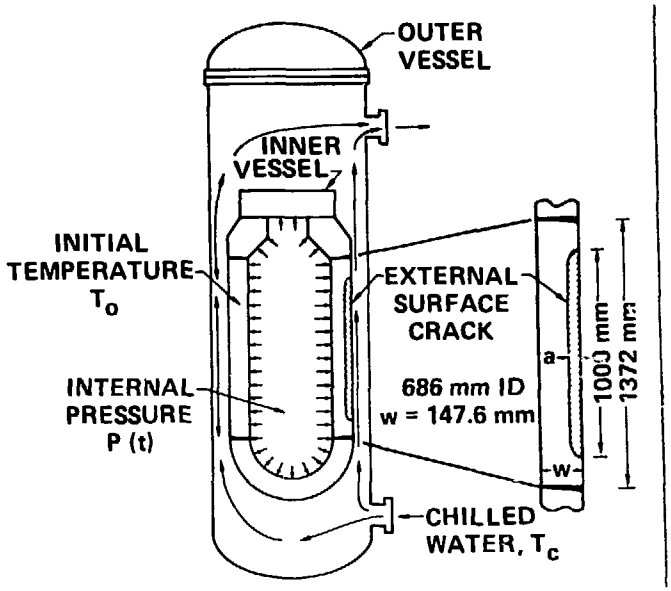

Fig. 13. Schematic of a pressurized-thermal-shock test vessel enclosed in an outer vessel.

heat transfer from the test vessel for a period of about 10 min. Pressurization of the test vessel is controlled independently by a system capable of pressures up to about 100 MPa.

Extensive material properties tests and fracture analyses preceded the transient test of the PTSE-1 vessel. The initial 1-m-long by 12.2-mm-deep flaw was axially oriented on the outside (cooled) surface of the vessel in a plug of specially tempered steel that would, with normal heat treatment, meet the specifications for SA-508 class 2 forging steel. The transient test was performed in three phases; in each phase the vessel was initially in an isothermal state (~290°C). Each phase consisted of a pressure transient and a thermal transient, which were coordinated to produce an evolution of stress and toughness states that would fulfill the objectives of the plan. Fracture analyses performed to define the transients were based on fracture-toughness data from tests of small specimens. Much of the run-arrest portions of the expected crack jumps in PTSE-1 would take place in a temperature range above that for which the small specimens could provide data; consequently, the transients were selected to attain the desired objectives in the presence of uncertainty. The ORMGEN/ADINA/ORVIRT system [21-23] of finite-element computer programs was used in conjunction with the OCA/USA program [27] to define the fracture properties and test transients.

The 1-m-long sharp flaw was implanted by cracking a shallow electron-beam weld under the influence of hydrogen charging. The vessel was extensively instrumented to give direct measurements of crack-mouth opening displacement.

Fracture initiation and arrest toughnesses were determined from tests of 25 mm and 37 mm compact specimens, respectively. Exponential expressions were fit to small specimen data to provide a basis for OCA/USA analysis of experiments in which the temperatures of interest were considerably higher than the temperature range of the small specimen tests. Thus, expressions similar to Eqs. (1) and (2) were used for K_{Ic} and K_{Ia}:

$$K_{Ic} = 51.276 + 2.2 \exp (0.036\ T) \tag{6}$$

and

$$K_{Ia} = 35 + 4.0177 \exp (0.02408\ T) \tag{7}$$

where the units for K_{Ic} and K_{Ia} are MPa$\cdot\sqrt{m}$ and T is in °C. Other details of material properties and the geometry of the test vessel are given in Refs. [28 and 29].

4.2 TEST RESULTS

The planned pressure transients for the three phases (A, B, and C) are shown in Fig. 14. If the material properties and the A transient had been precisely as desired, all of the objectives of the experiment might have been attained in that transient. However, because of inhibiting effects of warm prestressing, the crack did not propagate during the A transient, although K_I reached a maximum of 154 MPa$\cdot\sqrt{m}$, and the K_I/K_{Ic} ratio reached a maximum value of 2.1. Plans for the B and C transients were based upon the evidence from test phase A that the vessel was tougher (about 11%) than originally estimated and that, to overcome warm prestressing, a higher K_I value would have to be attained. Accordingly, the K_{Ic} expression used in pretest analyses was modified [to Eq. 6)] to agree with the results of the A transient, lower coolant temperatures were specified for the thermal transient [28], and a higher pressure transient was selected (curve B, Fig. 14). Unlike PTSE-1A, a two-step pressure transient was not performed during PTSE-1B because a second pressure increase of a useful magnitude was not within the capabilities of the pressurization system. The B transient resulted in a crack jump to a depth of 24.4 mm. The final transient, PTSE-1C, was performed under more severe thermal conditions [28] with the planned pressure transient described by curve C in Fig. 14. The crack jumped to a depth of 41 mm.

The flawed region was cut from the vessel, chilled in liquid nitrogen, and broken apart to reveal the fracture surfaces. Fractographic examination of the surfaces and measurement of the flaw geometry indicated that the initial flaw tore slightly prior to the initial cleavage fracture. The initial

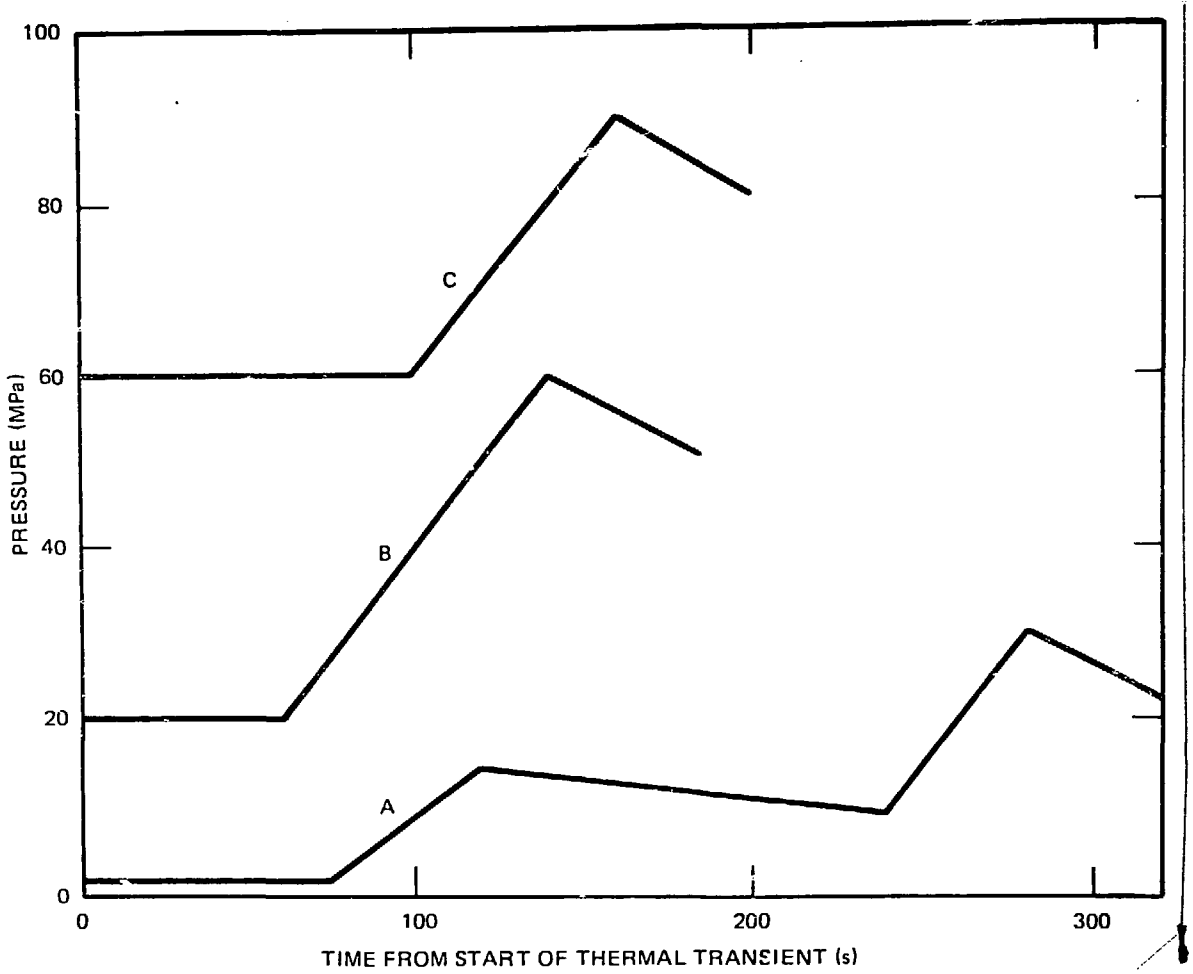

Fig. 14. Planned pressure transients for PTSE-1A, -1B and -1C.

crack extension was essentially a pure cleavage fracture throughout the first half of the extension and predominantly cleavage (~90%) with finely dispersed ductile tearing in the remaining portion of this extension. The crack extension in the second crack jump was mixed mode throughout with about 85% cleavage. At the ends of the two crack extensions there were no coherent regions of ductile tearing, contrary to predictions based on the measured tearing resistance J_R of the material.

After the propagation and arrest in PTSE-1B and -1C, the pressure continued to be increased, causing a further increase in K_I but without crack propagation. Initiation and arrest toughnesses from quasistatic calculations based on the experimental transient data are summarized in Table 4. The values of K_{Ic} and K_{Ia} inferred from the experiment are shown in Fig. 15 in comparison with the pretest estimates and the K_{Ic} and K_{Ia} relationships from Section XI of the ASME Boiler and Pressure Vessel Code. Pretest estimates of fracture toughness are reasonably close to the PTSE-1 values.

Table 4. Summary of fracture conditions in PTSE-1

Experiment phase	Event	Crack tip temperature (°C)	K_I (MPa·√m)
PTSE-1B	Initiation	104	177
	Arrest	163	201
	Subsequent max K_I	118	247
PTSE-1C	Initiation	125	254
	Arrest	179	299
	Subsequent max K_I	156	340

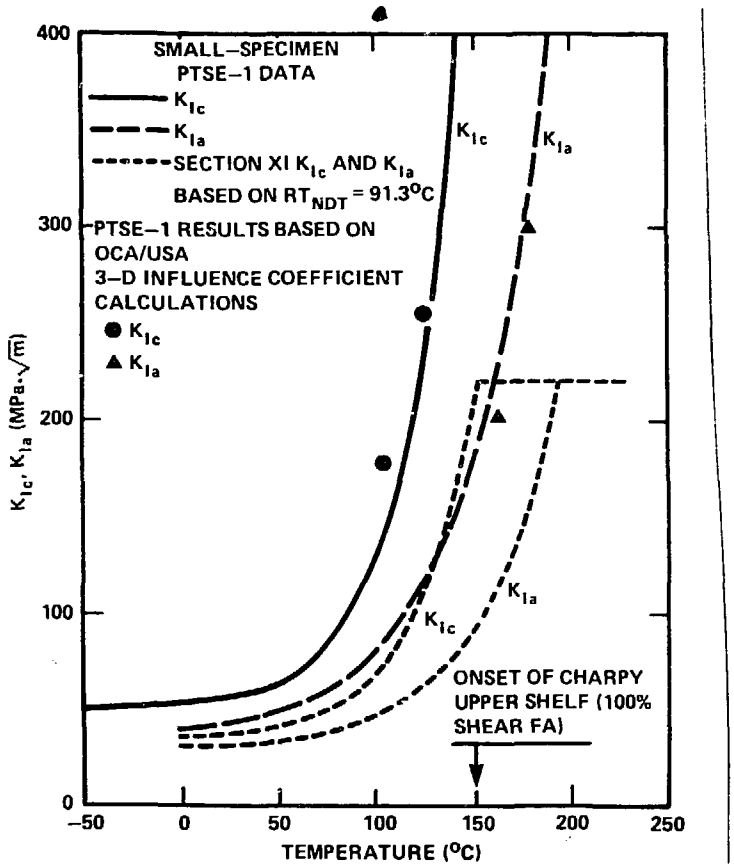

Fig. 15. Comparison of PTSE-1B and -1C results with curves representing small-specimen K_{Ic} and K_{Ia} data and ASME Section XI curves.

Dynamic analyses similar to those discussed earlier for the wide-plate tests were also performed. The dynamic properties used are those given by Eqs. (2) - (5), with RT_{NDT} = 91.3°C. The calculated crack-depth vs time is compared in Fig. 16 to the final crack depth for each run-arrest event. Additional results are given in Ref. [28].

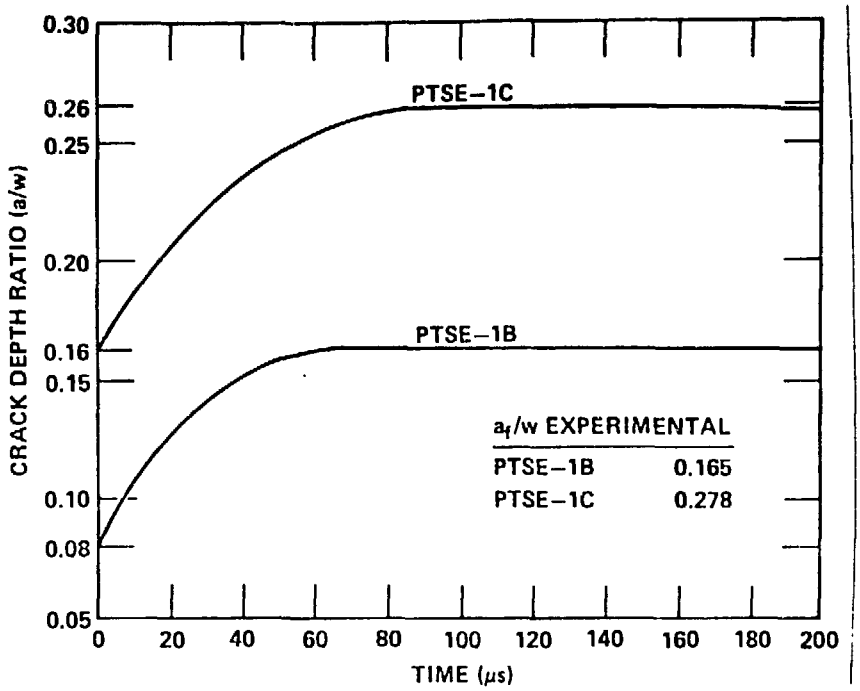

Fig. 16. Crack-depth ratio (a/w) vs time for posttest elastodynamic analysis of PTSE-1.

4.3 DISCUSSION

The first pressurized-thermal-shock experiment is a basis for quantitative conclusions regarding initiation and arrest toughnesses for one reactor vessel grade steel. Results from test data indicate that the ASME Boiler and Pressure Vessel Code Section XI toughness relations are conservative relative to actual material characteristics. The experiment demonstrated that arrest toughness substantially above the 220 MPa$\cdot\sqrt{m}$ cutoff of Section XI could be realized. Furthermore, the highest PTSE-1 value of arrest occurred at a temperature about 30 K above the onset of the Charpy upper shelf. This is believed to be very close to the threshold temperature above which cleavage fracture cannot persist. This result also suggests that the methods of linear elastic fracture mechanics have an important role in fracture evaluation at high (upper-shelf) temperatures. Further, Fig. 17 shows that the PTSE-1 data combine with the data from the wide-plate tests and from other large specimen experiments to form a consistent trend with $(T - RT_{NDT})$. The three other sources of data in Fig. 17 are discussed in Refs. [30-32].

The PTSE-1A and -1B transients demonstrate that simple warm prestressing ($\dot{K}_I < 0$) strongly inhibits crack initiation. With allowance for uncertainty in the true K_{Ic} values, it was evident that K_I exceeded K_{Ic} during warm prestressing by 20-90%. In transient A, simple antiwarm prestressing

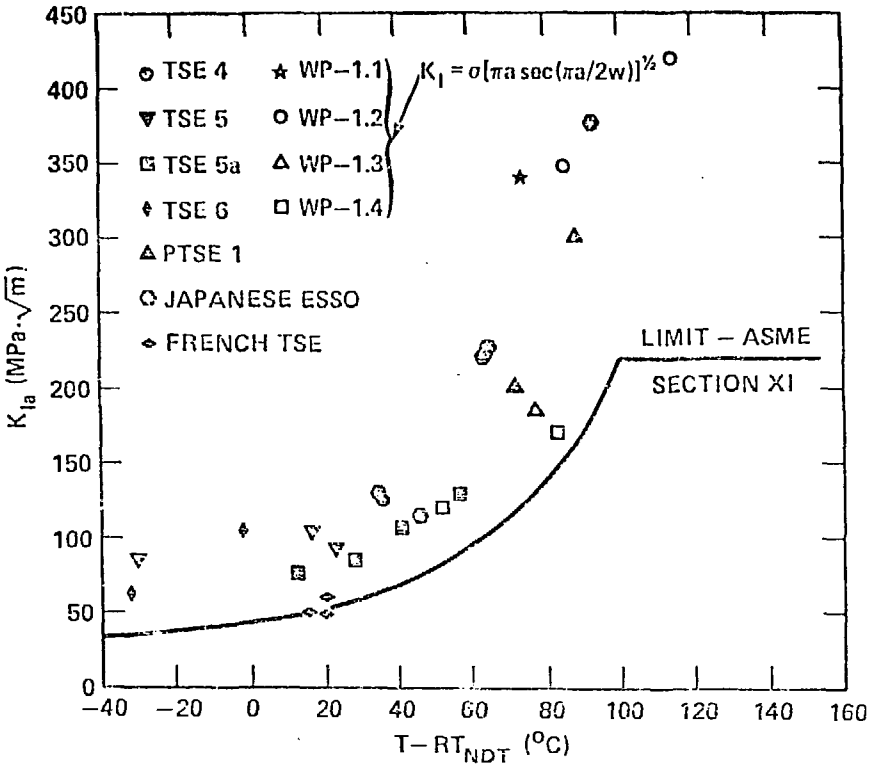

Fig. 17. The wide-plate and PTSE-1 crack-arrest data form a consistent trend with data from other large crack-arrest specimen tests.

($\dot{K}_I > 0$) prevailed during two periods of 40 s and 60 s duration without crack initiation, although K_I exceeded K_{Ic} by 70–90%. Clearly simple antiwarm prestressing ($\dot{K}_I > 0$) is not a sufficient condition to alleviate the effects of warm prestressing.

5. CONCLUSIONS AND RECOMMENDATIONS

The conclusions drawn from these studies suggest that procedures used for evaluating overcooling accidents in pressurized-water reactors should realistically take into consideration the structural considerations and fracture mechanisms that have been demonstrated but not yet generally accepted. Account should be taken of the presence of cladding and of the inhibiting effect of simple warm prestressing. Furthermore, it is not premature to allow consideration of crack-arrest toughness values above the 220 MPa·√m ceiling suggested in Section XI of the ASME Code. This consideration is supported not only by the observation that the K_{Ia} data from the wide-plate tests and PTSE-1 extend above the ASME limit, but also by observing that these data are consistent with those from other large-specimen experiments.

The above measures would make evaluations less conservative without being unrealistic. In a change toward conservatism, the phenomenon of ductile tearing below dynamic upper-shelf temperatures should be explicitly considered in vessel evaluations to ensure that the procedure is never nonconservative. This is because ductile tearing can precede the onset of cleavage if the tearing resistance is less than K_{Ic}. Some allowance for a decrease in initiation toughness with crack-tip strain rate caused by crack-front motion may also be necessary under these circumstances. Viscoplastic constitutive models are presently being considered for this purpose.

Posttest elastodynamic analysis results have shown good agreement with data for the short crack runs of PTS experiments, and static and dynamic analyses showed little difference. It is reasonable that dynamic effects are more pronounced in longer crack-run events that could accompany axial extension of a short flaw in a pressure vessel.

6. ACKNOWLEDGMENTS

The authors acknowledge Materials Engineering Associates, particularly J. R. Hawthorne, for cladding capsule fabrication and irradiation. They also express recognition of the large and dedicated efforts of R. deWit, R. J. Fields et al. of the National Bureau of Standards, Gaithersburg, MD, in performing and reducing the data from the HSST wide-plate crack-arrest tests. Appreciation is expressed to T. N. Jones, H. Blevins, G. C. Robinson, S. E. Bolt, H. D. Curtis, W. F. Jackson and T. M. Cate for experimental assistance. The contributions and guidance of G. D. Whitman, Head of the ORNL Pressure Vessel Technology Section, were invaluable throughout these investigations. They gratefully acknowledge the support and guidance of the HSST technical monitor, Milton Vagins, at the U.S. Nuclear Regulatory Commission.

7. REFERENCES

[1] W. R. Corwin, *Assessment of Radiation Effects Relating to Reactor Pressure Vessel Cladding*, NUREG/CR-3671 (ORNL/6047), Oak Ridge National Laboratory, Martin Marietta Energy Systems, Inc. (July 1984).

[2] W. L., Fourney, G. R. Irwin, and R. Chona, "ASTM Round Robin on K_{Ia} Testing," *Heavy-Section Steel Technology Program Semiannual Progress Report for April–September 1984*, NUREG/CR-3744, Vol. 2 (ORNL/TM-9154/V2), Oak Ridge National Laboratory, Martin Marietta Energy Systems, Inc.

[3] R. E. Cheverton et. al., "Fracture Mechanics Data Deduced from Thermal-Shock and Related Experiments with LWR Pressure Vessel Material," *Journal of Pressure Vessel Technology*, Vol. 105, May 1983, pp. 102-110.

[4] R. H. Bryan et. al., "The Heavy-Section Steel Technology Pressurized-Thermal-Shock Experiment, PTSE-1," submitted to *Engineering Fracture Mechanics* for publication, (1985).

[5] C. E. Pugh, "Crack Arrest Technology," *Heavy-Section Steel Technology Program Semiannual Progress Report for April-September 1984*, NUREG-CR-3744, Vol. 2 (ORNL/TM-9154/V2), Oak Ridge National Laboratory, Martin Marietta Energy Systems, Inc.

[6] G. C. Robinson et al., "Stainless Steel Cladding Investigations," *Heavy-Section Steel Technology Program Quarterly Progress Report for Period October-December 1982*, NUREG/CR-2751 Vol. 4 (ORNL/TM-8369/V4), Oak Ridge National Laboratory, Martin Marietta Energy Systems, Inc., pp. 133-138.

[7] W. R. Corwin et al., *Effect of Stainless Steel Weld Overlay Cladding on the Structural Integrity of Flawed Steel Plates in Bending, Series 1*, NUREG/CR-4015 (ORNL/TM-9390), Oak Ridge National Laboratory, Martin Marietta Energy Systems, Inc. (April 1985).

[8] W. R. Corwin, R. G. Berggren and R. K. Nanstad, "Charpy Toughness and Tensile Properties of a Neutron-Irradiated Stainless Steel Submerged-Arc Weld Cladding Overlay," *Effects of Irradiation Materials*: Twelth Conf. ASTM STP 870, (to be published).

[9] W. R. Corwin et al., "Stainless Steel Cladding Investigations," *Heavy-Section Steel Technology Program Quarterly Progress Report for Period January-March 1983*, NUREG/CR-3334, Vol. 1 (ORNL/TM-8787/V1), Oak Ridge National Laboratory, Martin Marietta Energy Systems, Inc., pp. 143-156.

[10] D. T. Read et al., "Metallurgical Factors Affecting the Toughness of 316L SMA Weldments at Cryogenic Temperatures," *Weld. J.* (Miami) 59(4) (1980) 104-113-s.

[11] F. W. Bennett and C. P. Dillon, "Impact Strength of Austenitic Stainless-Steel Welds at -320°F — Effects of Composition, Ferrite Content and Heat Treatment," *J. Basic Eng.* 88(3) (1966) 33-36.

[12] G. M. Goodwin, *Fracture Toughness of Austenitic Stainless Steel Weld Metal at 4 K*, ORNL/TM-9172, Oak Ridge National Laboratory, Martin Marietta Energy Systems, Inc. (August 1984).

[13] E. B. Norris, D. R. Ireland, and C. E. Lautzenheiser, *The Second Inspection of the Elk River Pressure Vessel After Operation*, SWRI-122, Southwest Research Institute Report (July 21, 1967).

[14] T. Kondo, H. Nakajima, and R. Nagasaki, "Metallographic Investigation of the Cladding Failure in the Pressure Vessel of a BWR," *Nucl. Eng. Design* 16 (1971) 205-122.

[15] J. R. Hawthorne and H. E. Watson, "Exploration of the Influence of Welding Variables on Notch Ductility of Irradiated Austenitic Stainless Steel Welds," *Proceedings of the International Conference on Radiation Effects in Breeder Reactor Structural Materials* (June 1977) pp. 327-336.

[16] B. R. Bass, C. E. Pugh, and H. K. Stamm, "Dynamic Analyses of a Crack Run-Arrest Experiment in a Nonisothermal Plate," in *Pressure Vessel Components Design and Analysis*, Vol. 4, ASME PVP Vol. 98-2, 1985.

[17] H. K. Stamm, B. R. Bass, and C. E. Pugh, *Fracture Analysis of Plate Crack Arrest Specimens*, Oak Ridge National Laboratory, Martin Marietta Energy Systems, Inc. (Report in preparation),

[18] A. R. Rosenfield et al., "Crack-Arrest Studies at Battelle Columbus," *HSST Program Semiannual Progress Report April-September 1984*, NUREG/CR-3744 Vol. 2, (ORNL/TM-9154/V2), pp. 102-109, Oak Ridge National Laboratory, Martin Marietta Energy Systems, Inc.

[19] D. P. Edmonds and J. J. McGowan, "Characterization of Wide-Plate Test Material at ORNL," *HSST Program Semiannual Progress Report for April-September 1984*, NUREG/CR-3744, Vol. 2 (ORNL/TM-9154/V2), pp. 96-102, Oak Ridge National Laboratory, Martin Marietta Energy Systems, Inc.

[20] M. F. Kanninen et al., *Preliminary Analysis of Japanese Wide Plate Dynamic Crack Propagation Arrest Experiments*, Subcontract report from Battelle Columbus Laboratories to Oak Ridge National Laboratory, December, 1983.

[21] B. R. Bass and J. W. Bryson, *Applications of Energy Release Rate Techniques to Part-Through Cracks in Plates and Cylinders, Vol. 1. ORMGEN-3D: A Finite-Element Mesh Generator for 3-Dimensional Crack Geometries*, NUREG/CR-2997, Vol. 1 (ORNL/TM-8527/V1), Oak Ridge National Laboratory, Martin Marietta Energy Systems, Inc. (December 1982).

[22] K. J. Bathe, *ADINA - A Finite Element Program for Automatic Dynamic Incremental Nonlinear Analysis*, Report 82448-1, Massachusetts Institute of Technology, Cambridge, MA, September 1975 (revised December 1978).

[23] B. R. Bass and J. W. Bryson, *Applications of Energy Release Rate Techniques to Part-Through Cracks in Plates and Cylinders, Vol. 2. ORVIRT: A Finite Element Program for Energy Release Rate Calculations for 2-D and 3-D Crack Models*, NUREG/CR-2997, Vol. 2 (ORNL/TM-8527/V2), Oak Ridge National Laboratory, Martin Marietta Energy Systems, Inc. (February 1983).

[24] H. Tada, P. C. Paris and G. R. Irwin, *The Stress Analysis of Cracks Handbook*, Del Research Corp., Hellertown, PA, 1973.

[25] C. F. Fedderson, "Current Status of Plain Strain Crack Toughness Testing of High-Strength Metallic Materials," ASTM STP-410, *Amer. Soc. Test. Materials* (1967).

[26] G. R. Irwin, *Notes on Testing Arrangements for Crack Arrest Tests Using an SEN Specimen and a Temperature Gradient*, University of Maryland, College Park, MD, private communication to C. E. Pugh (October 1983).

[27] R. H. Bryan and J. G. Merkle, "Upper-Shelf-Arrest Analysis Based on J_R-Controlled Tearing," *Heavy-Section Steel Technology Program Quart. Prog. Rep. January-March 1983*, NUREG/CR-3334, Vol. 1 (ORNL/TM-8787/V1), pp. 111-124, Oak Ridge National Laboratory, Martin Marietta Energy Systems, Inc. (September 1983).

[28] R. H. Bryan et al., "The Heavy-Section Steel Technology Pressurized-Thermal-Shock Test, PTSE-1," *J. Engrg. Fracture Mech.* 1985.

[29] R. H. Bryan et al., *Pressurized-Thermal-Shock Test of 6-in.-Thick Pressure Vessels, PTSE-1*, NUREG/CR-4106 (ORNL-6135), Oak Ridge National Laboratory, Martin Marietta Energy Systems, Inc. (April 1985).

[30] R. D. Cheverton et al., "Fracture Mechanics Data Deduced from Thermal-Shock and Related Experiments With LWR Pressure Vessel Material," *J. Pressure Vessel Technology, ASME*, Vol. 105 (1983).

[31] Japan Welding Council, *Structural Integrity of Very Thick Steel Plate for Nuclear Reactor Pressure Vessels*, JWES-AE-7806, 1977 (in Japanese).

[32] A. Pellissier-Tanon, P. Sollogoub, and B. Houssin, "Crack Initiation and Arrest in an SA 508 Class-3 Cylinder Under Liquid Nitrogen Thermal-Shock Experiment," Paper G/F 1/8, *Transactions of the 7th International Conference on Structural Mechanics in Reactor Technology*, Vols. G and H, 137-42 (August 1983).

DISCLAIMER